Medicinal chemistry

Ying et al., Med chem (Los Angeles) 2016, 6:3
DOI: 10.4172/2161-0444.1000342

Research Article Open Access

# Insight into the Mutation-Induced Decrease of the Enzymatic Activity of Human Cytochrome P450 1A2

**Bei-Li Ying[1,4], Bo-Tao Fa[2], Shan Cong[3], Yang Zhong[1*] and Jing-Fang Wang[2,4*]**

[1]*School of Life Sciences, Fudan University, Shanghai 200433, China*
[2]*Key Laboratory of Systems Biomedicine (Ministry of Education), Shanghai Center for Systems Biomedicine, Shanghai Jiao Tong University, Shanghai 200240, China*
[3]*College of Life Sciences and Biotechnology, Shanghai Jiao Tong University, Shanghai 200240, China*
[4]*Shanghai Center for Bioinformation Technology, Shanghai 201203, China*

## Abstract

As an important member of CYP1 sub-family, CYP1A2 mediates the metabolisms of approximately 5-10% of the currently clinical medicines, and plays a predominant role in the activation of precarcinogens. F186L mutation in this CYP enzyme is found to have ability to reduce the enzymatic activity. As this mutation is far away from the active site and has no influence on the protein expression, the detailed mechanism for F186L-induced the decrease of the enzymatic activity of CYP1A2 is still unknown. In the current study, we employed molecular dynamics simulation and free energy calculation to study the wild-type and F186L mutant CYP1A2 with a α-naphthoflavone (ANF) bound in the active site. Our simulations showed that instead of changing the backbone structure, the F186L mutation has significant impact on the side-chain conformations, resulting in a smaller active site and larger solvent accessible surface. The former could weaken the binding affinity of ANF in the active site, making the substrate far away from the active site so as to reduce the enzymatic activity. The latter could keep the substrate access channel in a closed state in most case, which was not propitious for the substrate entering into the active site by the substrate access channel. Our findings can reveal an in-depth understanding for the mechanism of the mutation-induced decrease of the enzymatic activity of human CYP1A2, providing useful information on the structure-function relationships of human CYP enzymes.

**Keywords:** Cytochrome P450 1A2; Decreased enzymatic activity; Molecular dynamics simulation; Structural analysis; Free energy calculation

**Abbreviations:** CYP1A2: Cytochrome P450 1A2; SNP: Single Nucleotide Polymorphism; ANF: α-naphthoflavone; MD: Molecular Dynamics; MM-PB/SA: Molecular Mechanics Poisson-Boltzmann Surface Area; MM-GB/SA: Molecular Mechanics Generalized Born Surface Area; SASA: Solvent Accessible Surface Area; RMS: Root-Mean-Square.

## Introduction

Cytochrome P450 (officially abbreviated as CYP) is a large and diverse group of enzymes belonged to the super-family of mono-oxygenases and heme-containing proteins [1,2]. These CYP enzymes are distributed in almost all kinds of organisms, i.e., animals, plants, fungi, bacteria, and even viruses [3,4]. CYP enzymes are so named by reason that the heme pigment contained therein absorbs a light at a wavelength of 450 nm after forming a complex with carbon monoxide. In mammalians, these CYP enzymes are primarily membrane-associated proteins located in either the endoplasmic reticulum or the inner membrane of the mitochondria of cells [5]. Mammalian CYP enzymes are able to oxidize both xenobiotics and endogenous compounds, which is believed to be significant for the detoxification of exogenous substances and the control of the endogenous compounds levels. In humans, CYP enzymes act as major metabolic enzymes with responsibility for phase I drug metabolism, accounting for ~ 90% of the clinical medicines [6]. CYP enzymes are also notable for their single nucleotide polymorphisms, which is estimated to affect nearly 20% of the clinical drug therapies [7,8].

Human cytochrome P450 1A2 (CYP1A2) is an important member of the CYP1 family in the CYP superfamily [9], and is predominantly expressed in the liver cells and at low levels in intestine, pancreas, lung as well as brain. In humans and most mammalians, family only contains 3 well characterized CYP enzymes: CYP1A1, CYP1A2 and CYP1B1. Although constituting nearly 13% of the total CYP content in hepatic tissues, CYP1A2 can mediate the metabolisms of approximately 5-10% of the currently clinical medicines [10]. Notably, CYP1A2 functions to mediate the metabolic reactions of caffeine, melatonin and marketed drugs, i.e., flutamide, lidocaine, tacrine and triamterene. Additionally, this CYP enzyme plays a predominant role in the activation of precarcinogens, including aromatic and heterocyclic amines as well as polycyclic aromatic hydrocarbons [11,12]. According to the recent evidences, the activation, overexpression and dysfunction of human CYP1A2 can lead to comparatively high risks of cancers [13-15].

By now, 16 defined alleles or single nucleotide polymorphisms (SNPs) of human CYP1A2 have been identified, as summarized in Table 1. From Table 1, it is found that 8 alleles or SNPs can significant decrease the enzymatic activity of human CYP1A2, among which CYP1A2*11 shows the most profound and statistically significant reduction in O-deethylation of phenacetin and 7-ethoxyresorufin [16]. As reported, the O-deethylation reaction rates mediated by this allele of phenacetin and 7-ethoxyresorufin reduce to 13% and 28% of the wild-type, respectively [16]. The CYP1A2*11 allele exhibits a clinically-relevant SNP in exon 2, resulting in a substitution on the amino acid sequence from phenylalanine to leucine at position 186 (F186L). This mutation (F186L) is located on the flexible loop between D and E helices far away from the catalytic center, and has no influence on the protein expression. Additionally, Phe186 in the wild-type CYP1A2 is found to be conserved among the CYP enzymes of the CYP1 family,

***Corresponding authors:** Yang Zhong, School of Life Sciences, Fudan University, Shanghai 200433, China, Tel: (86)21-3420-7344; Fax: (86)21-3420-7344; E-mail: yangzhong@fudan.edu.cn

Jing-Fang Wang, Key Laboratory of Systems Biomedicine (Ministry of Education), Shanghai Center for Systems Biomedicine, Shanghai Jiao Tong University, Shanghai 200240, China, E-mail: jfwang8113@sjtu.edu.cn

**Received** February 26, 2016; **Accepted** March 08, 2016; **Published** March 10, 2016

**Citation:** Ying BL, Fa BT, Cong S, Zhong Y, Wang JF (2016) Insight into the Mutation-Induced Decrease of the Enzymatic Activity of Human Cytochrome P450 1A2. Med chem (Los Angeles) 6: 174-178. doi:10.4172/2161-0444.1000342

| Allele | Nucleotide Changes | AA Mutations | Location | Enzymatic Activity Changes | Population | References |
|---|---|---|---|---|---|---|
| *CYP1A2*2* | 63C>A | F21L | Exon 2 | — | Chinese | [33] |
| *CYP1A2*3* | 2385G>A, 5347T>C | D348N | Exon 4 | Decreased | French | [34] |
| *CYP1A2*4* | 2499A>T | I386F | Exon 5 | Decreased | French | [34] |
| *CYP1A2*5* | 3497G>A | C406Y | Exon 6 | — | French | [35] |
| *CYP1A2*6* | 5090C>T | R431W | Exon 7 | Decreased | French | [34] |
| *CYP1A2*7* | 3533G>A | — | Intron 6 | Decreased | Caucasian | [36] |
| *CYP1A2*8* | 5166G>A, 5347T>C | R456H | Exon 7 | Decreased | Japanese | [37] |
| *CYP1A2*9* | 248C>T | T83M | Exon 2 | — | Japanese | [16] |
| *CYP1A2*10* | 502G>C | E168Q | Exon 2 | — | Japanese | [16] |
| *CYP1A2*11* | 558C>A | F186L | Exon 2 | Decreased | Japanese | [16] |
| *CYP1A2*12* | 634A>T | S212C | Exon 2 | — | Japanese | [16] |
| *CYP1A2*13* | 1514G>A | G299S | Exon 3 | — | Japanese | [16] |
| *CYP1A2*14* | 5112C>T | T438I | Exon 7 | Normal | Japanese | [16] |
| *CYP1A2*15* | 125C>G, 5347T>C | P42R | Exon 2 | Decrease | Japanese | [37] |
| *CYP1A2*16* | 2473G>A, 5347T>C | R377Q | Exon 5 | Decrease | Japanese | [37] |

**Table 1:** The alleles or single nucleotide polymorphisms (SNPs) of human CYP1A2.

and believed to play an essential role to maintain the normal catalytic functions of human CYP1A2.

In the current study, we focused on the problem why F186L mutation in human CYP1A2 can significantly reduce the enzymatic activity. To achieve this goal, we employed molecular dynamics simulations and free energy calculations to study the dynamic behaviors of both wild-type and F186L mutated CYP1A2, as well as their complexes with α-naphthoflavone (ANF). Molecular dynamics simulation can provide useful information for characterizing the internal motions of proteins or enzymes, as well as the interactions with ligands, giving structural insights for both basic research and drug development in the relevant area [17-20]. In comparison with the crystal studies, molecular dynamics simulation and free energy calculation have the advantages of analyzing the conformational fluctuations of CYP1A2 and the dynamic interactions with ANF.

## Materials and Computational Methods

### Starting structures of the wild-type and F186L mutated CYP1A2

The starting structure of the wild-type CYP1A2 was derived from the crystal structure 2hi4.pdb from the RCSB Protein Data Bank, which was released in February 20, 2007 with a resolution of 1.95 Å [21]. The F186L mutation structure was then constructed based on the wild-type structure using the coordinate reconstruction approach [22]. Except for the polar hydrogen and heavy atoms, all the other atoms in the simulation systems were removed. The pKa values for each residue were calculated by using Delphi as a Poisson-Boltzmann solver with a dielectric constant of 4.0 [23]. The removed hydrogen atoms were then added to the wild-type and F186L mutation structures with the t-Leap procedure packaged in Amber 11 [24] based on the computational pKa values mentioned above, to give a total charge of +6. Subsequently, all the simulation systems were solvated in a rectangular simulation box with explicit TIP3P water molecules. To neutralize the simulation systems, 6 chloride ions were added to random replace equal numbers of water molecules in the simulation box. The atoms of the wild-type and F186L mutation structures were parameterized by Amber force field parameters and the ones in the heme group were treated by the parameters obtained from previous QM/MM studies [25].

### Docking procedure to get the ANF-bound wild-type and F186L mutated CYP1A2

Before the docking procedure, 10 configurations of the wild-type and F186L mutated CYP1A2 were randomly selected from the simulation trajectories of the corresponding substrate-free systems. ANF was subsequently docked into the active site of all these configurations mentioned above using AutoDock 4.0 [26]. For each configuration, 1,000 independent runs were performed using genetic algorithms on a 55-Å cubic grid, centered on the geometrical center of the active site with a grid spacing of 0.375 Å. The binding modes with the lowest binding energy and favorably positioned ANF for O-deethylation among all the configurations were selected as the starting structures of the ANF-bound states of the wild-type and F186L mutated CYP1A2 for the further molecular dynamics simulation and free energy calculation.

### Molecular dynamics simulation

For the ANF-bound simulation systems, the ANF molecules were parameterized by Amber force field parameters using the antechamber module in Amber 11.28 After solvation, all the simulation systems were subjected to steepest descent energy minimization for about 3,000 steps, followed by conjugate gradient for the next 3,000 steps. Subsequently, all the simulation systems were equilibrated with the protein, heme group and ANF atoms fixed by a short-time molecular dynamics simulation to reduce the van der Waals conflicts. Finally, 14-ns molecular dynamics simulations were performed with the normal temperature (310 K), periodic boundary conditions and NPT ensemble. The SHAKE algorithm [27,28] with a tolerance of $10^{-6}$ was applied to constrain all the bonds in the simulation systems involving hydrogen atoms, and atom velocities for the start-up runs were derived according to the Maxwell distribution at 310 K [29,30]. For each simulation system, 10 independent simulations were carried out with different start-up velocities. The isothermal compressibility was set to $4.5\times10^{-5}$/bar for the solvent simulations. The electrostatic interactions were treated by particle mesh Ewald (PME) algorithm with interpolation order of 4.0 and a grid spacing of 0.12 nm. The van der Waals interactions were calculated by using a cut-off of 12 Å. All the molecular dynamics simulations were performed with a time step of 2 fs, and the coordinates for all the simulation systems were saved every 1 ps.

### Free energy calculation

The molecular mechanics Poisson-Boltzmann surface area (MM-PB/SA) [31] and molecular mechanics Generalized-Born surface area (MM-GB/SA) [32] methods implemented in Amber 11 was applied to calculate the binding free energy for the ANF-bound wild-type and F186L mutated CYP1A2. The principles of the MM-PB/SA and MM-GB/SA methods can be summarized as following:

$$\Delta G_{bind} = G_{complex} - \left(G_{protein} + G_{ligand}\right) \quad (1)$$

$$G \cong E_{gas} - TS_{config} + G_{sol} \quad (2)$$

$$E_{gas} = E_{bond} + E_{angle} + E_{torsion} + E_{vdw} + E_{ele} \quad (3)$$

$$G_{sol} = G_{ele} + G_{non-polar} \quad (4)$$

In equation 1, the binding free energy change ($\Delta G$) is calculated as the difference between the free energies of the complex ($G_{complex}$), the protein ($G_{protein}$) as well as the ligand ($G_{ligand}$). These free energies are computed through equation 2 by summing up its internal energy in the gas phase ($E_{gas}$), the solvation free energy ($G_{sol}$), and a vibrational entropy term ($TS$). As the systems involved in our study have similar entropy, the entropy contributions are neglected with an aim of comparisons of the free energy differences for the active substrate between single-ligand binding and cooperative binding systems. $E_{gas}$ is a standard force field energy calculated from equation 3 by the strain energies from covalent bonds ($E_{bond}$ and $E_{angle}$) and torsion angles ($E_{torsion}$), non-covalent van der Waals ($E_{vdw}$), and electrostatic energies ($E_{ele}$). As described in equation 4, the solvation free energy ($G_{sol}$) is computed by both an electrostatic term ($G_{ele}$) and a non-polar component ($G_{non-polar}$). The former can be obtained from either the Possion-Boltzman method (PB) or the Generalized Born (GB) method. The latter is considered to be proportional to the molecular solvent accessible surface area (SASA). In the current study, a total 200 snapshots retrieved from the last 1-ns segment on the simulation trajectories with an interval of 5 ps were used for the binding free energy calculations [33-37].

## Results and Discussion

### Molecular dynamics trajectory analysis

There are totally 4 simulation systems involved in the current study, denoted as the substrate-free wild-type, the substrate-free F186L mutation, the ANF-bound wild-type and ANF-bound F186L mutation, respectively. As the root-mean-square (RMS) deviation is thought to be a crucial criterion to evaluate the convergence of the simulation systems, we first calculated the RMS deviation values for the backbone structures of all the simulation systems. As shown in Figure 1A, the RMS deviation values for all the simulation systems employed minor changes from the starting structures, and no significant RMS deviation fluctuations were detected. The final RMS deviation values for all the simulation systems were not more than 2.5 Å from the corresponding starting structures, giving an indication that these simulation systems were equilibrated. This observation also supported that the F186L mutation did not lead to remarkably large-scale structural motions for the entire protein.

Addition to the RMS deviation analysis, we also calculated the RMS fluctuation values for each residue in the wild-type and F186L mutant structures. As shown in Figures 1B and 1C, in general the F186L mutant structure was more flexible than the wild-type. Significant fluctuations on the F186L mutant structure with respect to the wild-type structure were detected to be located on D helix and the loops between D and E helices, E and F helices as well as G and H helices. The F186L mutation was located on the loop between D and E helices near the protein surface (Figure 2), and the substitution from the aromatic side-chain to the aliphatic one could lead to some kind of instability in aqueous solution. Thus, it was expected that the mutant structure employed structural fluctuations or more flexibility in the nearby regions. However, these structural fluctuations did not change the overall structure of the protein, or at least the backbone structure.

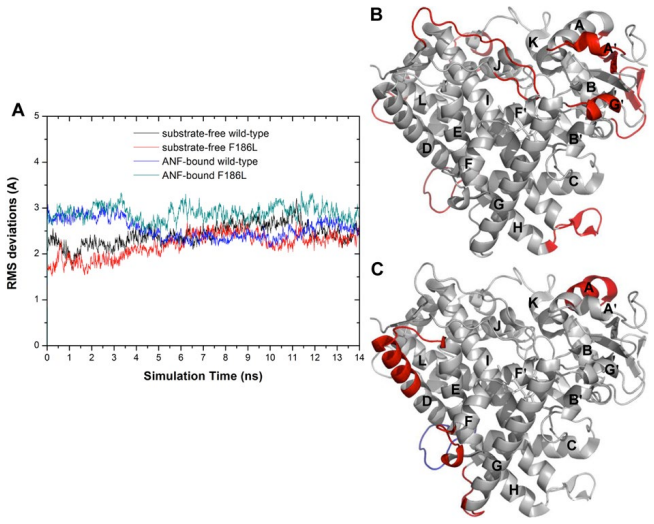


**Figure 1:** RMS deviations and fluctuations of the backbone structure of human CYP1A2. (A) Time-dependent RMS deviations values for both wild-type and F186L mutant structures along molecular dynamics trajectories. (B) Illustratively showing the highlight regions with significant RMS fluctuations (>1 Å, colored in red) on the wild-type structure. (C) Illustratively showing the highlight regions with significant RMS fluctuations (>1 Å, colored in red; <-1 Å, colored in blue) on the F186L mutant structure with respect to the wild-type structure.

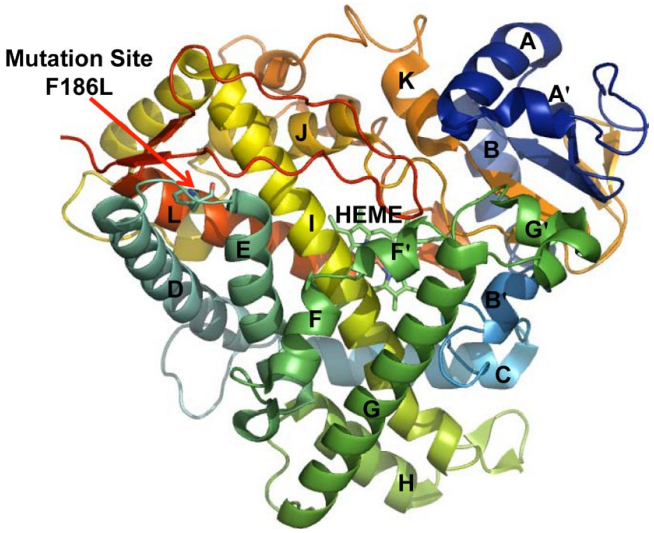


**Figure 2:** The overall three-dimensional structure of human CYP1A2. The F186L mutation was located on the loop between D and E helices on the protein surface. This mutation had little impacted on the entire protein structure, and could increase the flexibility of CYP1A2.

### Conformational changes between the wild-type and F186L mutant CYP1A2

According to the molecular dynamics trajectory analysis mentioned above, the major distinctions between the wild-type and mutant structures were found only around the mutation (F186L), indicating that the mutation did not change the backbone structure of the entire protein. Instead, F186L mutation probably had significant influences on the side-chain conformation, especially for some key residues. To support this view, we firstly calculated the solvent accessible surface area (SASA) for both the wild-type and F186L mutation based on 100 snapshots retrieved from the last 1-ns segment on the molecular

dynamics trajectories with an interval of 10 ps. The total SASA value for the wild-type was ~ 22955.0 ± 101.7 $nm^3$, significantly smaller than that of the F186L mutation (23235.8 ± 103.4 $nm^3$, T-test P value <0.05). Besides, it was also found that the hydrophobic SASA value contributed most to the total SASA, which for the wild-type (11478.5 ± 99.4 $nm^3$) was also significantly smaller than that of the mutant structure (11619.3 ± 98.1 $nm^3$, T-test P value <0.05). This observation indicated that the side-chain conformation of the mutant structure was quite different from that of the wild-type.

Additionally structural analyses showed that the SASA variances between the wild-type and F186L mutation might be caused by the notably structural motions around D and E helices. In the wild-type structure, the aromatic side-chain of Phe186 (located on the loop between D and E helices) could form a π-π stacking interaction with Phe481 (located on the loop after L helix in the C-terminal region). This π-π stacking interaction was able to position the flexible loop region in the C-terminal, which was also a key component for the substrate access channel (Figure 3). The substitution from phenylalanine to leucine at position 186 would break the significant π-π stacking interaction mentioned above, resulting in the unlocking the C-terminal loop regions, which would be more flexible. The flexible loop in the C-terminal region would further impact on the substrate access channel. In the wild-type structure, the diameter in the narrowest part of the substrate access channel was 3.41 ± 0.60 Å, much larger than that in the mutant structure (2.86 ± 0.68 Å). This observation showed that the substrate access channel in the mutant structure were in a closed state in most cases, which was not propitious for the substrate entering into the active site by the substrate access channel.

## Free energy calculations

To further study the influence of F186L mutation on the substrate binding, we also estimated the binding free energies using both MM-PB/SA and MM-GB/SA methods. The computational results were summarized in Table 2. The binding free energies for ANF in the wild-type structure were -8.52 ± 3.22 kcal/mol (obtained from MM-PB/SA approach) and -10.67 ± 1.89 kcal/mol (obtained from MM-GB/SA approach), which were much lower than those in the F186L mutant structure (-6.27 ± 3.17 kcal/mol obtained from MM-PB/SA approach and -8.41 ± 1.65 kcal/mol obtained from MM-GB/SA approach). Based on the energy term analysis, the variations of the binding free energies for the wild-type and F186L mutant structures were mainly focused on the electrostatic energies ($\Delta E_{ele}$) and van der Waals interactions ($\Delta E_{vdw}$). The former for the wild-type and F186L mutant structures were -3.86 ± 1.81 kcal/mol and -3.32 ± 1.92 kcal/mol, respectively. The latter for the wild-type and F186L mutant structures were -15.37 ± 1.79 kcal/mol and -13.50 ± 1.41 kcal/mol, respectively.

After observing the molecular dynamics trajectories, we found that the ANF binding site in the wild-type and F186L mutant structures were quite different (Figure 4). In the wild-type structure, the ANF binding site was close to the heme group, which was propitious to the further metabolic reactions of ANF. In the F186L mutant structure, the ANF binding site was comparatively far away from the heme group. This was mainly because that the active site pocket in the F186L mutant structure became smaller. So, we used 100 snapshots retrieved from the last 1-ns segment on the molecular dynamics trajectories with an interval of 5 ps to calculate the active site volume of the wild-type and F186L mutant CYP1A2. The active site volume for the wild-type structure was 178 ± 29 $Å^3$, much larger than that of the F186L mutant structure (93 ± 30 $Å^3$). As mentioned above, the smaller active site volume in the F186L mutant structure was mainly caused by the conformational changes of the side-chains.

| Energies terms | Wild-type | F186L mutation |
|---|---|---|
| $\Delta E_{ele}$ | -3.86 ± 1.81 | -3.32 ± 1.92 |
| $\Delta E_{vdw}$ | -15.37 ± 1.79 | -13.50 ± 1.41 |
| $\Delta E_{gas}$ | -19.23 ± 3.64 | -16.82 ± 3.02 |
| $\Delta G_{non\text{-}polar/PB}$ | -1.84 ± 0.09 | -1.80 ± 0.10 |
| $\Delta G_{ele/PB}$ | 12.55 ± 2.74 | 12.35 ± 2.44 |
| $\Delta G_{sol/PB}$ | 10.71 ± 2.65 | 10.55 ± 2.38 |
| $\Delta G_{bind/PB}$ | -8.52 ± 3.22 | -6.27 ± 3.17 |
| $\Delta G_{non\text{-}polar/GB}$ | -2.48 ± 0.10 | -2.56 ± 0.15 |
| $\Delta G_{ele/GB}$ | 11.04 ± 1.94 | 10.97 ± 1.96 |
| $\Delta G_{sol/GB}$ | 8.56 ± 2.09 | 8.41 ± 1.85 |
| $\Delta G_{bind/GB}$ | -10.67 ± 1.89 | -8.41 ± 1.65 |

Note: $\Delta E_{gas}=\Delta E_{ele}+\Delta E_{vdw}$; $\Delta G_{sol/PB}=\Delta G_{ele/PB}+\Delta G_{non\text{-}polar/PB}$; $\Delta G_{bind/PB}=\Delta E_{gas}+\Delta G_{sol/PB}-T\Delta S$; $\Delta G_{bind/GB}=\Delta E_{gas}+\Delta G_{sol/GB}-T\Delta S$

**Table 2:** Binding free energies (kcal/mol) calculated by the MM-PB/SA and MM-GB/SA methods for ANF bound in the wild-type and F186L mutated CYP1A2.

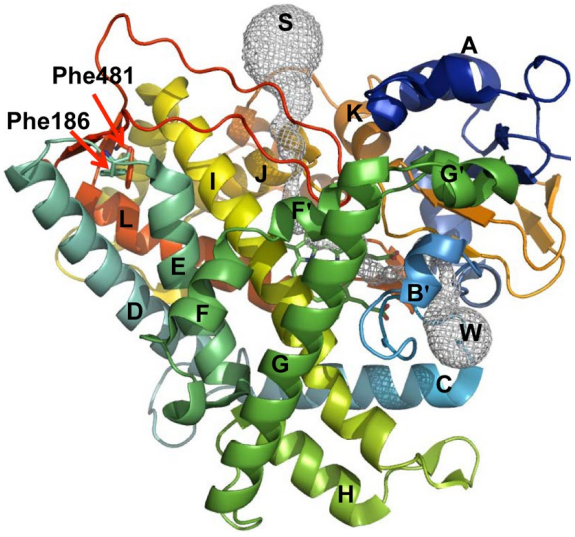


**Figure 3:** Illustratively showing the π-π stacking interaction between side-chains of Phe186 and Phe481. This π-π stacking interaction could lock the loop region after L helix in the C-terminal region. The F186L mutation could break this π-π stacking interaction, making the loop region mentioned above more flexible.

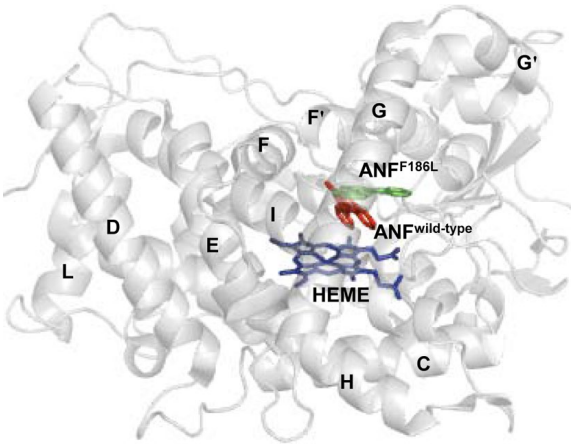


**Figure 4:** ANF binding modes in the wild-type and F186L mutant structures. In the wild-type structure, the ANF binding site (colored in red) was close to the heme group, which was propitious to the further metabolic reactions of ANF. In the F186L mutant structure, the ANF binding site (colored in green) was comparatively far away from the heme group due to the much smaller active site volume.

## Conclusion

In the current study, we focused on human CYP1A2, which have 8 alleles that can significant decrease its enzymatic activity. Among the 8 alleles, CYP1A2*11 allele (F186L) was selected for further studies. This is because that this mutation is located on the flexible loop between D and E helices far away from the catalytic center, and has no influence on the protein expression. To understand why this mutation can significant decrease the enzymatic activity of human CYP1A2, we performed molecular dynamics simulation and free energy calculation on both wild-type and F186L mutant CYP1A2 with a ANF bound in the active site. Our molecular dynamics trajectories showed that this mutation had little influence on the entire protein structure. Instead, this mutation impacted on the side-chain conformations. As a result, the F186L mutant structure employed a smaller active site and larger solvent accessible surface. The former could weaken the binding affinity of ANF in the active site, while the latter made the substrate access channel in a closed state. Our findings can reveal an in-depth understanding for the mechanism of the mutation-induced decrease of the enzymatic activity of human CYP1A2, providing useful information on the structure-function relationships of human CYP enzymes.

### Acknowledgments

This work was supported by the grants from the National Natural Science Foundation of China (No. 31200547), Doctoral Program Foundation of Institutions of Higher Education of China (No. 20110073120078), and China Postdoctoral Science Foundation (No. 20110490068).

### References

1. Danielson PB (2002) The cytochrome P450 superfamily: biochemistry, evolution and drug metabolism in humans. Curr Drug Metab 3: 561-597.
2. Wang JF, Zhang CC, Chou KC, Wei DQ (2009) Structure of cytochrome p450s and personalized drug. Curr Med Chem 16: 232-244.
3. Nelson DR (1999) Cytochrome P450 and the individuality of species. Arch Biochem Biophys 369: 1-10.
4. Chen Q, Zhang T, Wang JF, Wei DQ (2011) Advances in human cytochrome p450 and personalized medicine. Curr Drug Metab 12: 436-444.
5. Wang JF, Chou KC (2010) Molecular modeling of cytochrome P450 and drug metabolism. Curr Drug Metab 11: 342-346.
6. Guengerich FP (2008) Cytochrome p450 and chemical toxicology. Chem Res Toxicol 21: 70-83.
7. Ingelman-Sundberg M (2005) The human genome project and novel aspects of cytochrome P450 research. Toxicol Appl Pharmacol 207: 52-56.
8. Ingelman-Sundberg M (2004) Pharmacogenetics of cytochrome P450 and its applications in drug therapy: the past, present and future. Trends Pharmacol Sci 25: 193-200.
9. Wang B, Zhou SF (2009) Synthetic and natural compounds that interact with human cytochrome P450 1A2 and implications in drug development. Curr Med Chem 16: 4066-4218.
10. Faber MS, Jetter A, Fuhr U (2005) Assessment of CYP1A2 activity in clinical practice: why, how, and when? Basic Clin Pharmacol Toxicol 97: 125-134.
11. Butler MA, Iwasaki M, Guengerich FP, Kadlubar FF (1989) Human cytochrome P-450PA (P-450IA2), the phenacetin O-deethylase, is primarily responsible for the hepatic 3-demethylation of caffeine and N-oxidation of carcinogenic arylamines. Proc Natl Acad Sci U S A 86: 7696-7700.
12. Eaton DL, Gallagher EP, Bammler TK, Kunze KL (1995) Role of cytochrome P4501A2 in chemical carcinogenesis: implications for human variability in expression and enzyme activity. Pharmacogenetics 5: 259-274.
13. Jernstrom H, Henningson M, Johansson U, Olsson H (2008) Coffee intake and CYP1A2*1F genotype predict breast volume in young women: implications for breast cancer. Br J Cancer 99: 1534-1538.
14. Cornelis MC, El-Sohemy A, Kabagambe EK, Campos H (2006) Coffee, CYP1A2 genotype, and risk of myocardial infarction. JAMA 295: 1135-1141.
15. Bugano DD, Conforti-Froes N, Yamaguchi NH, Baracat EC (2008) Genetic polymorphisms, the metabolism of estrogens and breast cancer: a review. Eur J Gynaecol Oncol 29: 313-320.
16. Murayama N, Soyama A, Saito Y, Nakajima Y, Komamura K, et al. (2004) Six novel nonsynonymous CYP1A2 gene polymorphisms: catalytic activities of the naturally occurring variant enzymes. J Pharmacol Exp Ther 308: 300-306.
17. Wang Y, Wei DQ, Wang JF (2010) Molecular dynamics studies on T1 lipase: insight into a double-flap mechanism. J Chem Inf Model 50: 875-878.
18. Wang JF, Chou KC (2011) Insights from modeling the 3D structure of New Delhi metallo-Î²-lactamse and its binding interactions with antibiotic drugs. PLoS One 6: e18414.
19. Li J, Wei DQ, Wang JF, Li YX (2011) A negative cooperativity mechanism of human CYP2E1 inferred from molecular dynamics simulations and free energy calculations. J Chem Inf Model 51: 3217-3225.
20. Wang JF, Chou KC (2012) Insights into the mutation-induced HHH syndrome from modeling human mitochondrial ornithine transporter-1. PLoS One 7: e31048.
21. Sansen S, Yano JK, Reynald RL, Schoch GA, Griffin KJ, et al. (2007) Adaptations for the oxidation of polycyclic aromatic hydrocarbons exhibited by the structure of human P450 1A2. J Biol Chem 282: 14348-14355.
22. Blundell TL, Sibanda BL, Sternberg MJ, Thornton JM (1987) Knowledge-based prediction of protein structures and the design of novel molecules. Nature 326: 347-352.
23. Georgescu RE, Alexov EG, Gunner MR (2002) Combining conformational flexibility and continuum electrostatics for calculating pK(a)s in proteins. Biophys J 83: 1731-1748.
24. Case DA, Cheatham TE 3rd, Darden T, Gohlke H, Luo R, et al. (2005) The Amber biomolecular simulation programs. J Comput Chem 26: 1668-1688.
25. Schoneboom JC, Lin H, Reuter N, Thiel W, Cohen S, et al. (2002) The elusive oxidant species of cytochrome P450 enzymes: characterization by combined quantum mechanical/molecular mechanical (QM/MM) calculations. J Am Chem Soc 124: 8142-8151.
26. Morris GM, Huey R, Lindstrom W, Sanner MF, Belew RK, et al. (2009) AutoDock4 and AutoDockTools4: Automated docking with selective receptor flexibility. J Comput Chem 30: 2785-2791.
27. Wang Y, Wu XL, Wei DQ, Li YX, Wang JF (2012) Autoinhibitory mechanism for the mutation-induced impaired FGF9 signaling. J Chem Inf Model 52: 2422-2429.
28. Liu Y, Liu BY, Hao P, Li X, Li YX, et al. (2013) Ï€-Ï€ Stacking mediated drug-drug interactions in human CYP2E1. Proteins 81: 945-954.
29. Wang YJ, Wang JF, Ping J, Yu Y, Wang Y, et al. (2012) Computational studies on the substrate interactions of influenza A virus PB2 subunit. PLoS One 7: e44079.
30. Zhang LS, Wang SQ, Xu WR, Wang RL, Wang JF (2012) Scaffold-based pan-agonist design for the PPARα, PPARβ and PPARγ receptors. PLoS One 7: e48453.
31. Wang JF, Hao P, Li YX, Dai JL, Li X (2012) Exploration of conformational transition in the aryl-binding site of human FXa using molecular dynamics simulations. J Mol Model 18: 2717-2725.
32. Chen LL, Wang JL, Hu Y, Qian BJ, Yao XM, et al. (2013) Computational design of glutamate dehydrogenase in Bacillus subtilis natto. J Mol Model 19: 1919-1927.
33. Huang JD, Guo WC, Lai MD, Guo YL, Lambert GH (1999) Detection of a novel cytochrome P-450 1A2 polymorphism (F21L) in Chinese. Drug Metab Dispos 27: 98-101.
34. Zhou H, Josephy PD, Kim D, Guengerich FP (2004) Functional characterization of four allelic variants of human cytochrome P450 1A2. Arch Biochem Biophys 422: 23-30.
35. Chevalier D, Cauffiez C, Allorge D, Lo-Guidice JM, Lhermitte M, et al. (2001) Five novel natural allelic variants-951A>C, 1042G>A (D348N), 1156A>T (I386F), 1217G>A (C406Y) and 1291C>T (C431Y)-of the human CYP1A2 gene in a French Caucasian population. Hum Mutat 17: 355-356.
36. Allorge D, Chevalier D, Lo-Guidice JM, Cauffiez C, Suard F, et al. (2003) Identification of a novel splice-site mutation in the CYP1A2 gene. Br J Clin Pharmacol 56: 341-344.
37. Saito Y, Hanioka N, Maekawa K, Isobe T, Tsuneto Y, et al. (2005) Functional analysis of three CYP1A2 variants found in a Japanese population. Drug Metab Dispos 33: 1905-1910.